Bioactive Materials 37 (2024) 239–252

Contents lists available at ScienceDirect

Bioactive Materials

journal homepage: www.keaipublishing.com/en/journals/bioactive-materials

ROS-responsive & scavenging NO nanomedicine for vascular diseases treatment by inhibiting endoplasmic reticulum stress and improving NO bioavailability

Jian Li [a,1], Jvhong Zhang [a,1], Pengcheng Yu [a,1], Han Xu [b], Meihui Wang [a], Zhebin Chen [a], Bo Yu [b], Jing Gao [a], Qiao Jin [b], Fan Jia [a,**], Jian Ji [b,*], Guosheng Fu [a,***]

[a] Key Laboratory of Cardiovascular Intervention and Regenerative Medicine of Zhejiang Province, Department of Cardiology, Sir Run Run Shaw Hospital, Zhejiang University, Hangzhou, 310016, PR China
[b] MOE Key Laboratory of Macromolecule Synthesis and Functionalization of Ministry of Education, Department of Polymer Science and Engineering, Zhejiang University, Hangzhou, PR China

ARTICLE INFO

Keywords:
Cardiovascular diseases
Nitric oxide
Reactive oxygen species
Endoplasmic reticulum stress
Nanomedicine

ABSTRACT

Vascular diseases seriously threaten human life and health. Exogenous delivery of nitric oxide (NO) represents an effective approach for maintaining vascular homeostasis during pathological events. However, the overproduction of reactive oxygen species (ROS) at vascular injury sites would react with NO to produce damaging peroxynitrite ($ONOO^-$) species and limit the therapeutic effect of NO. Hence, we design a ROS-responsive NO nanomedicine (t-PBA&NO NP) with ROS scavenging ability to solve the dilemma of NO-based therapy. t-PBA&NO NP targets NO and anti-oxidant ethyl caffeate (ECA) to the injury sites via collagen IV homing peptide. The ROS-triggered ROS depletion and ECA release potently alleviate local oxidative stress via ROS scavenging, endoplasmic reticulum and mitochondrial regulation. It subsequently maximizes vascular modulation effects of NO, without production of harmful compounds, reactive nitrogen species (RNS). Therefore, it significantly increases competitiveness of human umbilical vein endothelial cells (HUVECs) over human aortic smooth muscle cells (HASMCs) both in vitro and in vivo. The strategy proved effective in inducing faster re-endothelialization, inhibiting neointimal formation and restoring vascular homeostasis. The synergy between ROS depletion and NO therapy served as a new inspiration for the treatment of cardiovascular diseases and other ROS-associated illnesses.

1. Introduction

The high morbidity and mortality make cardiovascular diseases (CVD) the biggest killer of humans' lives and formidable threat to patients' health [1,2]. In the progression of CVD, the vascular injured sites are usually characterized by elevated local ROS level, subsequently accompanied by pathological vascular remodeling [3,4]. The dysfunction and lose of endothelium and overthickening of base-membrane eventually progress into lumen occlusion, which is the leading cause of heart failure and even death during CVD [5,6]. Therefore, restoration of the normal balance of vascular microenvironment after CVD occurrence proves vital in preventing subsequent lethal cardiovascular events, and is of great meaning in preserve patients' health and life [7–9].

In the innermost layer of blood vessels, a thin, single layer of cells forms the endothelium, which serves as the boundary between the circulating blood and underlying tissues [10]. More importantly, endothelium would produce many molecules as native signals to modulate the physiological vascular homeostasis [11,12]. Among them, NO is the most well-known endogenous signaling molecule with vast functions in cardiovascular system [13,14]. Produced by

Peer review under responsibility of KeAi Communications Co., Ltd.
* Corresponding author.
** Corresponding author.
*** Corresponding author.
E-mail addresses: jiafan@zju.edu.cn (F. Jia), jijian@zju.edu.cn (J. Ji), fugs@zju.edu.cn (G. Fu).
[1] These authors contributed equally: Jian Li, Jvhong Zhang, Pengcheng Yu.

https://doi.org/10.1016/j.bioactmat.2024.03.010
Received 21 December 2023; Received in revised form 21 February 2024; Accepted 8 March 2024

enzyme-catalyzed oxidation of arginine, NO is critical in preventing platelet aggregation, regulating smooth muscle cells' phenotype and maintaining endothelial cells' functions [15–18]. Under pathological conditions, the function and intactness of endothelium were compromised, leading to reduction in NO generation [19]. Therefore, supply exogenous NO donor would be a direct solution in regaining vascular balance in CVD.

However, the efficacy of NO-based therapies was seriously dampened by the high level of ROS in the microenvironment. Due to their high reactiveness, ROS not only consume NO, but also produce highly toxic species such as peroxynitrite ($ONOO^-$) [20–22]. The processes decreased NO bioavailability, while also aggravated endothelium injury and dysfunction. On the other hand, overwhelming ROS can also affect normal biological processes and interrupt endoplasmic reticulum (ER) activities. It induces accumulation of unfolded/misfolded proteins, retards metabolism of lipid and releases of calcium ions (Ca^{2+}) into the cytoplasm, which is generally termed as ER stress [23]. It may further cause the apoptosis of endothelial cells during CVD and wickedly help the progression of diseases [24,25].

Therefore, scavenging excessive ROS is not only beneficial in maximizing bio-effect of NO-based therapy, but also critical in regulating key steps of endothelium injury [26–28]. Nanomedicines have been widely studied for the treatment of CVD based on the protection of cells and tissues by direct or indirect ROS clearance [29,30]. For example, Wu and co-workers developed a ROS-consuming block copolymer poly(ethylene glycol) and poly(propylene sulfide) (PEG–PPS) loaded with andrographolide. This polymeric micelle had combined antioxidant capability and achieved a great therapeutic effect on atherosclerosis [31]. Previously, our group developed a new method to synthesize boronic acid esters [32–34]. Ethyl caffeate (ECA), a key ingredient of Chinese herb, has potent ability of relieving oxidative stress. The catechol structure of ECA readily reacts with boronic acid to yield correlated esters. Meanwhile, the obtained materials fast response to ROS stimuli, and spontaneously release the conjugated diols. The by-product 4-hydroxybenzyl alcohol can further eliminate ROS, as a potent anti-oxidant. Hence, these materials are desirable choices in oxidative stress related diseases and offer potential solution to the dilemma of NO-based CVD therapy.

Herein, a hydroxypropyl-β-cyclodextrin (HP-β-CD) based supramolecular drug scaffold was fabricated to achieve ROS-responsive ROS depletion and subsequent NO release. ECA based boronic acid ester was attached to HP-β-CD via standard 1,1′-carbonyldiimidazole (CDI) activation. The NO donor, isosorbide dinitrate (ISDN), was loaded into the cavity of HP-β-CD via host-guest interaction. We hypothesized that the nano-encapsulated supramolecular drugs could response and scavenge high level of ROS at sites of CVD-induced injury. The scavenging of ROS and release of ECA may help in relief of ER stress-related cellular disorder, and optimize condition for NO to exert broad bio-functions. A typical balloon-induced rat carotid artery injury model was adopted to evaluate the therapeutic effect, which may provide a new approach for the treatment of cardiovascular diseases (Fig. 1).

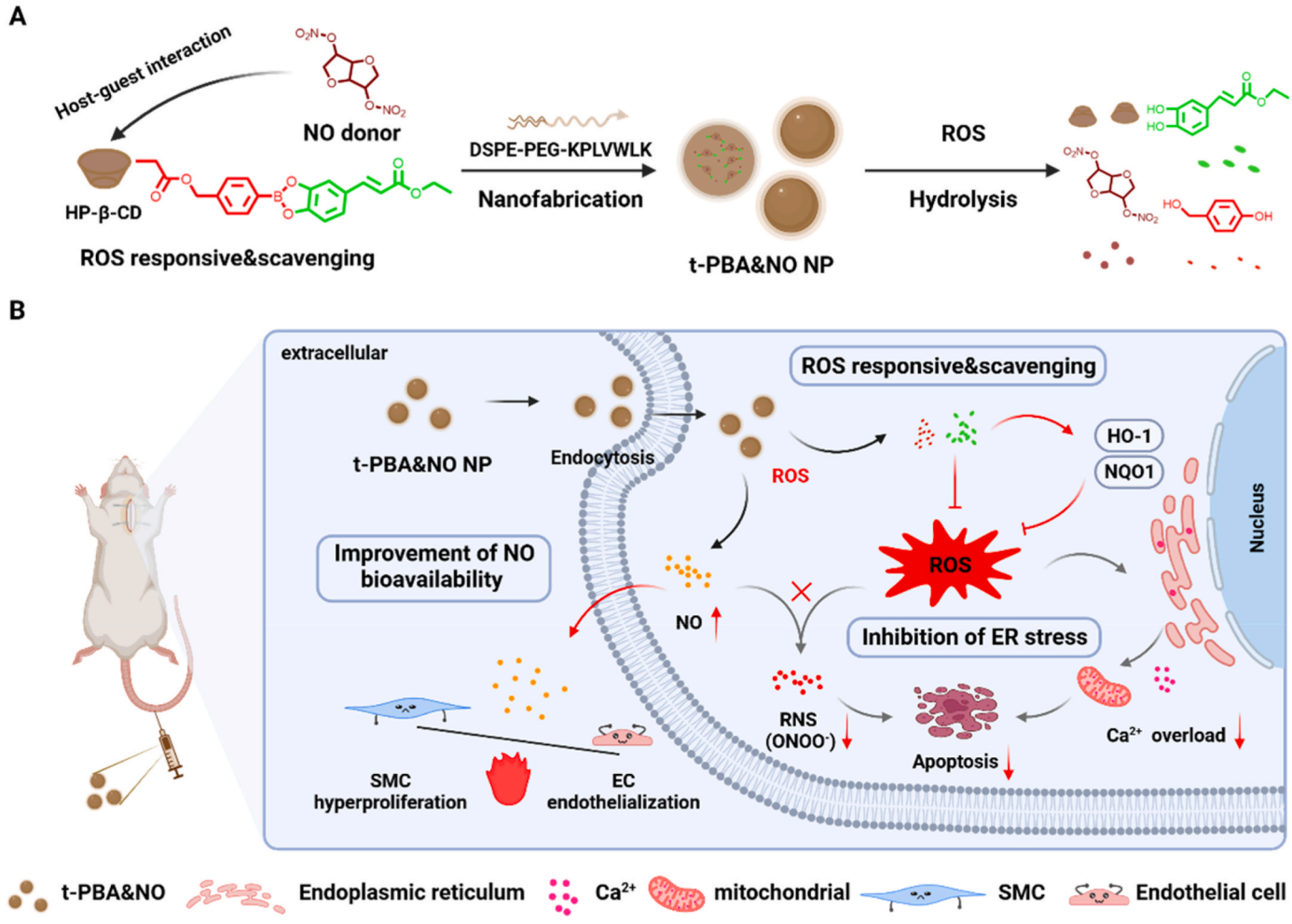

Fig. 1. Schematic illustration of ROS-responsive & scavenging nanomedicines for vascular injury diseases treatment. With excellent ROS-responsive & scavenging ability, nanomedicines can achieve exogenous delivery of NO while inhibiting the conversion of NO to $ONOO^-$ caused by elevated ROS, thereby improving the bioavailability of NO and providing a basis for the differential regulation of endothelial cells (ECs) and smooth muscle cells (SMCs). In addition, this nanomedicine will regulate the homeostatic imbalance of Ca^{2+} induced by ER stress and inhibit subsequent mitochondrial dysfunction and apoptosis.

2. Results and discussion

2.1. Synthesis, preparation and characterization of nanomedicines

HP-β-CD is a cyclodextrin derivate with excellent water solubility and low toxicity. It inherited the readiness of reaction and the potential as a host molecule of cyclodextrins. This HP-β-CD-based phenylboronic acid ethyl caffeate ester (β-CD-PBA) was prepared by a simple, efficient, one step process as previously described [32]. The quantitively yielded 4-(hydroxymethyl) phenylboronic acid ethyl caffeate ester (PBA) were then grafted onto HP-β-CD to obtain β-CD-PBA. NMR, UV–visible and FT-IR spectroscopy were employed to evaluate the conjugation of phenylborate ester onto the HP-β-CD (Fig. 2B–D). The average number of phenylborate ester attached to HP-β-CD was calculated as 2, based on the integrated area of the characteristic peaks of phenyl group at 7.3–7.7 ppm of 4-methylhydroxy phenylboronic acid and methylene group at 4.1 ppm of ECA in ^{1}H NMR spectrum. The characteristic absorption peak of phenylborate ester also emerged in the UV–vis spectrum of β-CD-PBA. Furthermore, in the FT-IR spectrum, the appearance of peaks at 1735 cm^{-1} and 1450-1600 cm^{-1} indicated the existence of the stretching vibration of the aldehyde group (C═O) of ECA and aromatic ring skeleton. All these results indicated the successful synthesis of β-CD-PBA.

The nanoparticles were prepared by a self-assembly/nanoprecipitation method following previously reported protocol [35]. To improve the nanomedicines' targeting ability, a type IV collagen (Col-IV) targeting peptide, CGGGKLWVLPK, was decorated on the DSPE-PEG by thiol-maleimide click chemistry (Fig. S1D). A non-targeting peptide with scrambled sequences, CGGGLKVPWKL, was used as contrast. In order to better elucidate the mechanism, the groups containing only NO or PBA was set up to explore its physiological effects, respectively. In addition, the characteristic peaks of ISDN (3.8–3.9 ppm) and HP-β-CD (5.4–5.5 ppm) are obviously correlated as shown by 2D ^{1}H NOSEY spectrum (Fig. S2), which indicated the occurrence of host-guest interaction.

The resulting nanoparticles demonstrated a spherical morphology and a narrow size distribution, which was confirmed by TEM and DLS (Fig. 2G), respectively. As shown in Fig. 2E–F, the hydrodynamic diameter and surface charge were measured by Zetasizer Nano-ZS. All nanomedicines had negative surface zeta potential of −3.7 ± 0.9 mV, −4.4 ± 2.9 mV, −5.0 ± 0.7 mV, and −3.9 ± 1.4 mV and similar hydrodynamic diameters of 132.1 ± 9.0 nm, 124.5 ± 7.5 nm, 114.9 ± 10.6 nm, and 152.6 ± 0.6 nm for NO NP, PBA NP, nt-PBA&NO NP, and t-PBA&NO NP, respectively. Unfortunately, we could not detect the NO signal after incubation with PBA or cell lysis for 24 h, possibly due to the enzymatic release nature of NO from ISDN in living organisms (Fig. S6). Under the stimulation of 1 mM H_2O_2, the 24-h cumulative drug release percentage of PBA&NO NP was 96.13 ± 0.06 % (Fig. 2H and Fig. S3). Our design of this nanomedicine could not only response to ROS stimulation but also scavenge excessive ROS afterwards. Therefore, the ROS scavenging ability was evaluated by DPPH assay and ABTS assay. PBA&NO NP demonstrated DPPH radical elimination in a dose-dependent manner (Fig. 2I). Similarly, the scavenged ABTS was increased with the dosage of PBA (Fig. 2J). Collectively, these results confirmed the ROS-scavenging ability of PBA&NO NP.

In conclusion, the preliminary results indicated that the nanoparticles with appropriate size, negative surface charge and ROS-responsive & scavenging capability were successfully prepared.

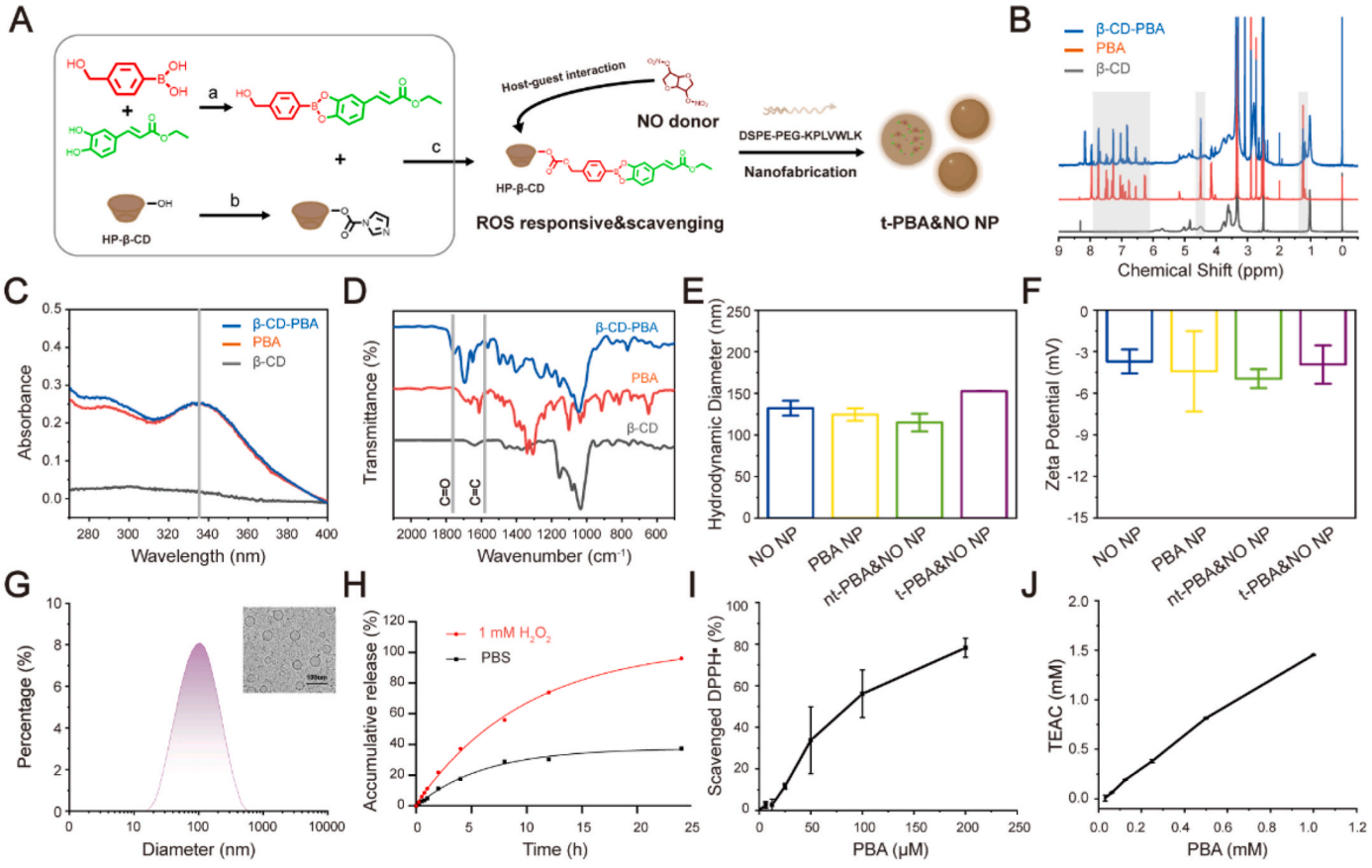

Fig. 2. Characterization of different NPs. (A) Schematic illustration of β-CD-PBA synthesis and t-PBA&NO fabrication. a, DMF, 100 °C, 8 h; b, CDI, DCM, 1 h; c, DMAP, DMF, 24 h. The ^{1}H NMR (B), UV–vis spectrum (C) and FT-IR (D) of β-CD-PBA, PBA, and β-CD. The intensity number (E) and zeta potential (F) of different nanoparticles. The hydrodynamic diameters (G) and TEM results (G, the inner image) of t-PBA&NO NP. Scale bar, 100 nm. (H) ROS-responsive 24-h release profiles of t-PBA&NO NP in PBS with or without H_2O_2. DPPH assay (I) and ABTS assay (J) of PBA&NO NP. Data are presented as mean ± SD (n = 3).

2.2. Regulation of oxidative stress of NPs on HUVECs

Since most oxidative stress-related damages originated inside cells, the uptake of nanomedicines was firstly evaluated. Coumarin-6 labeled NPs were co-cultured with HUVECs. The fluorescent intensity increased over time (Fig. S4), indicating continuous uptake of NPs by HUVECs. Quantification data from flow cytometry also yielded similar conclusion. The biocompatibility of NPs on HUVECs and HASMCs was then examined by CCK-8 assay (Fig. S5). Compared with control group, there were no significant changes in cell viability of the other groups, indicating that the different NPs showed good biocompatibility.

When the injury occurs, the ROS rich microenvironment exerts oxidative stress to endothelium, causing loss of intactness and functions. Without the native regulation, SMCs may overgrow and impair vascular

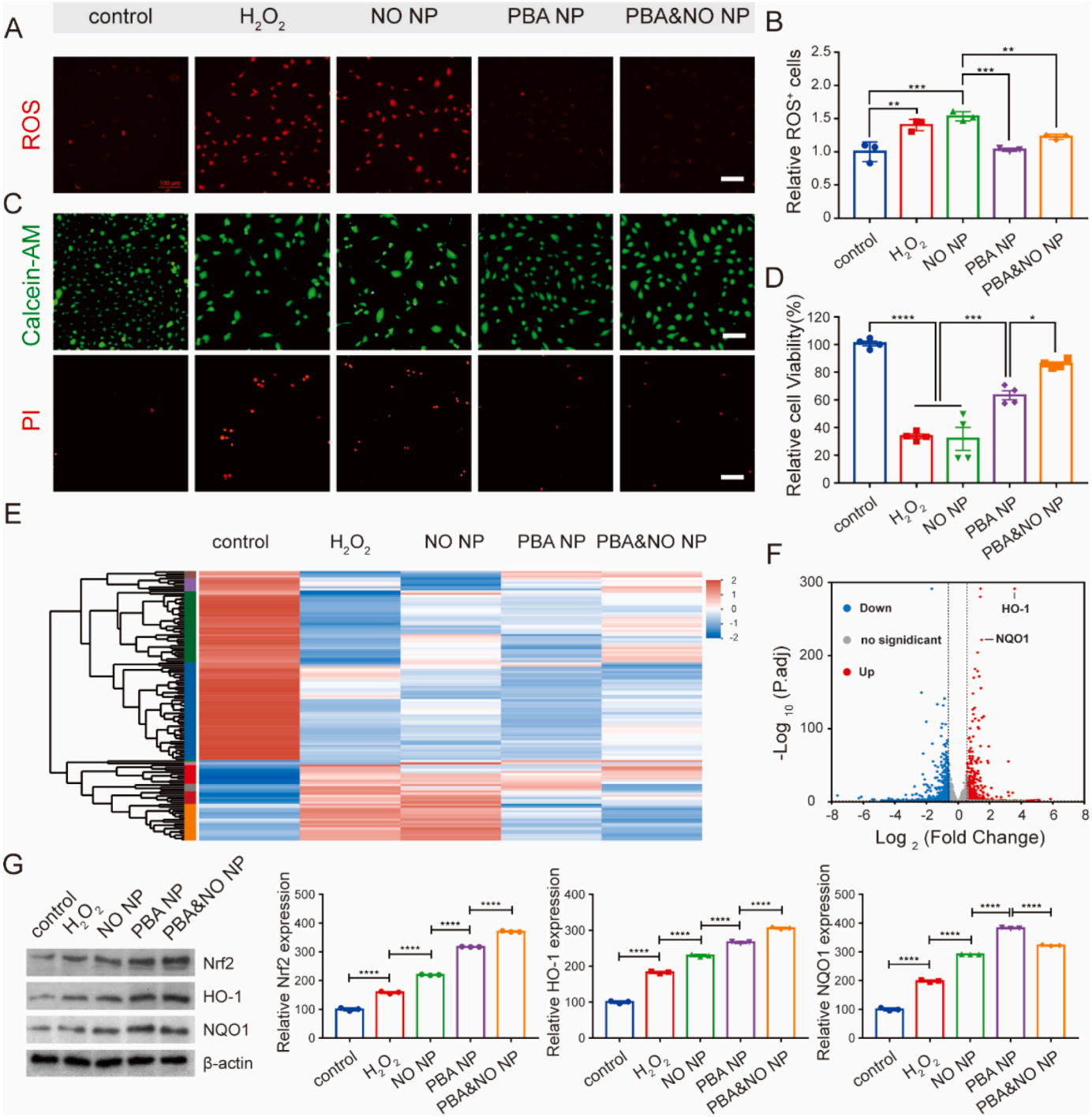

Fig. 3. Regulation of intracellular oxidative stress of NPs in HUVECs. Intracellular ROS level after different treatments (A) fluorescent images of cells co-cultured with DHE probe (scar bar, 100 μm) and (B) quantitative analysis by flow cytometry. (C) Live/dead staining results (Scale bars, 100 μm) after incubation with different treatments for 24 h. (D) Cell viability of HUVECs after incubation with different treatments for 24 h. (E) Heat map of differentially expressed genes (DEGs) in RNA-Seq results after different treatments. (F) Volcano plot of all genes from H_2O_2 and PBA&NO group. (G) WB bands and quantitative statistics of Nrf2, HO-1 and NQO1 expression after different treatments for 24 h. The concentrations of NO and PBA in the NPs were both 10 μM. Data in (D) are presented as mean ± SD (n = 4). Data in (B and G) are presented as mean ± SD (n = 3). *$p < 0.05$, **$p < 0.01$, ***$p < 0.001$, ****$p < 0.0001$.

homeostasis [5,11]. In vitro, this process was simulated by extra H_2O_2. To detect the ROS eliminating capacity of different NPs, DHE, a ROS responsive fluorescent probe, was used to visualize intracellular ROS levels. Red fluorescence intensity significantly increased in HUVECs treated with 500 μM H_2O_2 for 4 h (a surplus 40% as demonstrated by flow cytometry), compared with cells under normal cultivate conditions (Fig. 3A–B). NO NP treatment alone didn't change the intracellular ROS levels, demonstrating bright red fluorescence with similar intensity. However, PBA NP and PBA&NO NP showed potent ROS scavenging ability, with dimmer intracellular fluorescence after treatment, respectively. It indicated the HP-β-CD based ECA derivate was a desirable antioxidant.

Calcein-AM-PI staining assay and CCK-8 cell viability assay were also employed to evaluated the cellular protective effect on HUVECs under oxidative stress. As shown in Fig. 3C, the number of red fluorescent-positive dead cells significantly decreased in PBA NP and PBA&NO NP groups compared with the H_2O_2 treated group. Treatment of only NO NP couldn't protect cells from death. It is worth noting that the cell viability in PBA&NO NP group was restored to 86% of the control group, which was better than both PBA NP or NO NP only treatment (Fig. 3D). The results indicated potential synergetic effects between the antioxidant PBA and NO donors.

2.3. Protecting mechanism of NPs on HUVECs

Whole-transcriptome analysis by RNA sequencing (RNA-seq) was performed to further explore the pathways and mechanisms of NPs' protecting effects on HUVECs. When treated with 500 μM H_2O_2, most transcriptomes of HUVECs showed significant changes compared with the untreated control group. The differences were alleviated when H_2O_2 incubated cells were further treated with PBA or PBA&NO NPs. It is interesting that NO NP treatment alone did not reverse the transcription differences (Fig. 3E). Compared with H_2O_2 treated group, 722 genes were upregulated and 540 genes were downregulated in HUVECs after PBA&NO NP treatment (differentially expressed genes, or DEGs; defined using log2(FC) $>$ 1.0 and P. adj$<$0.05, respectively). Among them, the changes of HO-1 and NQO1 signaling pathways were the most significant ones. These proteins were related to the cellular self-defense against ROS damage. And the expression of HO-1 and NQO1 was up-regulated by 12.14 $\pm$ 0.87 and 2.87 $\pm$ 0.06 times, respectively (Fig. 3F). It seems to be related to the anti-oxidative stress effect of PBA&NO NP.

To verify this assumption, Western Blot assay was conducted on cell samples with different treatments. In consistence with the RNA-seq analysis, the protein level of HO-1 and NQO1 were significantly upregulated after different NPs treatment. The further promotion of these endogenous antioxidant proteins expression in PBA and PBA&NO NP groups was beneficial in preserving cell viability and normal functions (Fig. 3G). Besides, Nrf2, an upstream transcription factor, was also upregulated in a similar way. Nrf2 plays an important role in inducing endogenous antioxidant response, such as regulating redox balance, metabolism, autophagy, DNA repair and mitochondrial physiology [36,37]. All these results suggested that PBA&NO NP not only scavenging ROS themselves as described above, but also activating endogenous antioxidative pathways.

2.4. Regulation of the ER stress and mitochondrial-related cell apoptosis

Based on data from The Comparative Gene Ontology (GO) analysis and Kyoto Encyclopedia of Genes and Genomes (KEGG) pathway analysis, we further concluded that changes in ER stress, regulation of apoptotic process, cGMP-mediated signaling and regulation of cell proliferation were involved in the DEGs (Fig. 4A). These results also pointed to the pathways of ER stress, TNF and PI3K-Akt related signaling, which are all closely related to the activities of ER (Fig. 4B). ER is responsible for properly folding and processing polypeptide chains to functional proteins in cells [38,39]. Many exogenous or endogenous factors lead to the misfolded or unfolded proteins in ER, which will cause the abnormality of ER and subsequent calcium-efflux (Fig. 4C). According to the literatures, reducing mitochondrial ROS production by regulating intracellular calcium homeostasis and inhibiting mPTP opening could effectively inhibit cell damage [27,29,40].

Accordingly, cytoplasmic calcium was visualized by calcium-sensitive indicator, Fluo-4 AM. The results demonstrated that the fluorescence intensity of H_2O_2 treated group was significantly higher than that in the control group (Fig. 4D). PBA or PBA&NO NPs incubation reduced the cytoplasmic calcium correlated fluorescence intensity to the level similar with control group. But NO NP treatment alone had no effect. It demonstrated that anti-oxidant strategy rather than NO therapy is the cause behind ER stress relief.

Meanwhile, ER activities also influence several other organelles, with ER-mitochondrial interactions as one of the most characteristic examples. Calcium released from the ER may end up in neighboring mitochondria, which vitally regulates mitochondrial function, division, and apoptosis [41,42]. Therefore, the level of mitochondrial calcium was then evaluated by Rhod-2 AM and Mitotracker co-staining (Fig. 4E). After H_2O_2 treatment, Rhod-2 AM-related fluorescence in HUVECs were much brighter than that in normal cells. PBA NP or PBA&NO NP treatment remarkably reduced the probe fluorescence intensity, indicating that mitochondrial calcium overload was relieved. Decrease of mitochondrial membrane potential are highly associated with abnormality of mitochondria and cellular apoptosis. JC-10 assay was used to access mitochondrial membrane potential. Orange fluorescence from JC-10 aggregates indicated normal mitochondrial membrane potential and healthy mitochondria activity, while green fluorescence from JC-10 monomers indicated the contrary. As shown in Fig. 4F, the green fluorescence intensity significantly increased and the orange fluorescence intensity decreased in the H_2O_2 treated group, and NO therapy alone barely reversed the trend. However, PBA NP and PBA&NO NP treatment brought the H_2O_2 incubated cells back to normal. Furthermore, the extend of cell apoptosis was evaluated with Annexin V-FITC-PI assay by flow cytometry (Fig. 4G). NO NP treatment alone could not decrease the percentage of the apoptotic cells. But the introduction of PBA would change this situation and greatly reduce the proportion of apoptotic cells in both early and late stage. These results were also confirmed by WB results (Fig. 4H). The expression of anti-ER stress protein XBP1 and anti-apoptosis protein Bcl-2 demonstrated obvious elevation after PBA NP and PBA&NO NP treatments, while NO NP alone has limited effects. On the other hand, level of pro-apoptosis proteins of BAX and c-cas3 decreased by PBA NP and PBA&NO NP treatments, but not with NO NP incubation.

These results vividly demonstrated the therapeutic dilemma of NO in bio-applications under oxidative condition. It also proved that PBA conjugates were effective in relieving ROS-induced ER stress and subsequent mitochondria-related cell apoptosis via calcium modulation pathway, providing a mechanistic explanation for the protective effect on HUVECs.

2.5. Enhanced competitiveness of HUVECs over HASMCs by restoring NO bioavailability

In vessels, the ECs were vital in maintaining vascular homeostasis, keeping SMCs in check. The damage of endothelium will activate the aberrant proliferation of SMCs. It is essential to restore the intactness of ECs and simultaneously inhibit the overgrowth of SMCs. NO was the potent signaling molecule to realize such modulation. Yang and co-workers developed a local NO-generating coating on the vascular stent to reduce the neointimal hyperplasia and achieve rapid reendothelialization [43]. However, under oxidative stress microenvironment, NO tends to react with ROS to produce high toxic $ONOO^-$, causing extended injury and remarkable reduction in the bioavailability of NO.

To verify these assumptions, the level of NO and $ONOO^-$ inside cells were detected, respectively (Fig. 5A–C and S6). Bright green

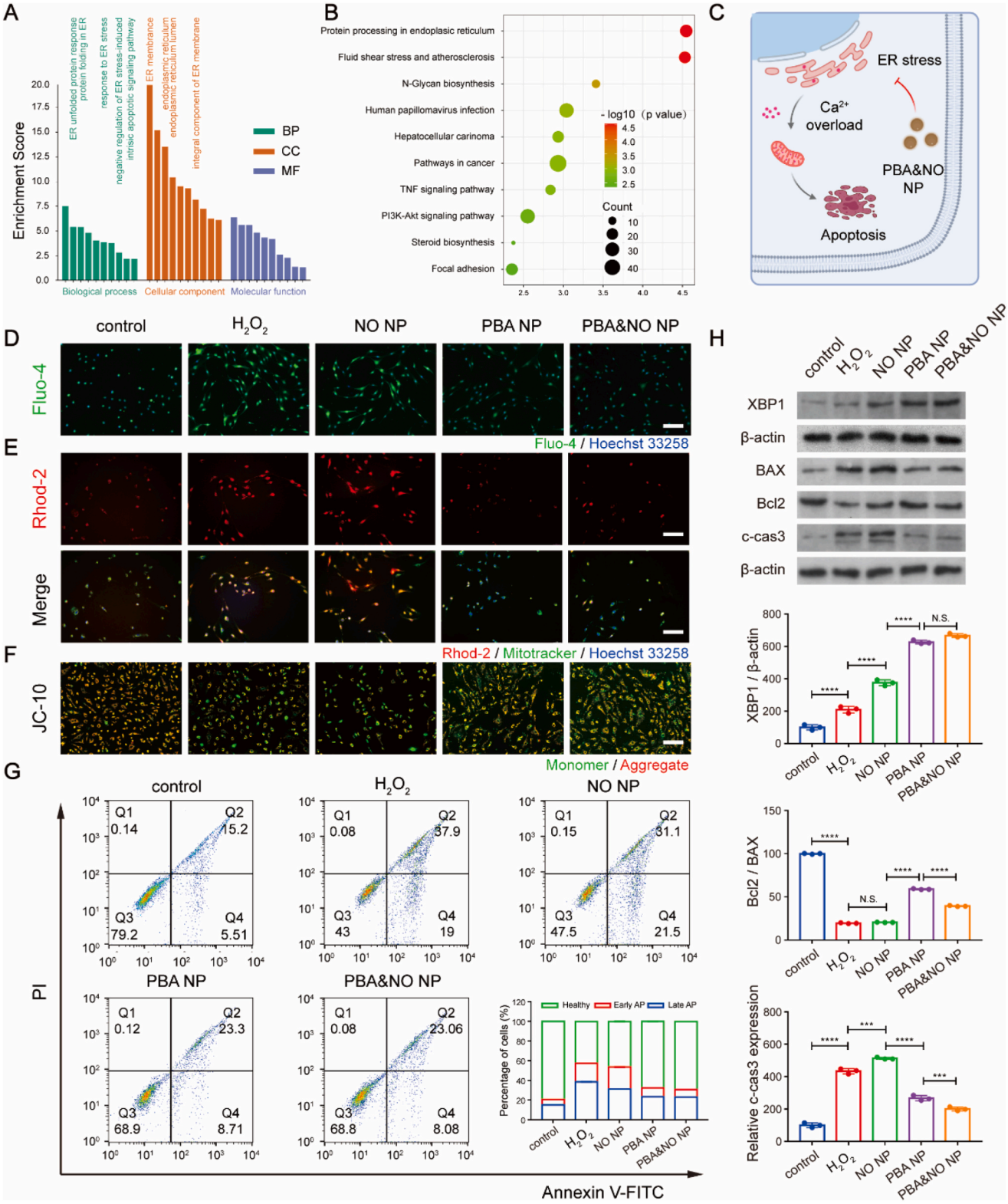

Fig. 4. Regulation of ER stress by NPs in HUVECs. (A) Gene ontology (GO) classification and (B) Kyoto Encyclopedia of Genes and Genomes (KEGG) pathway enrichment analysis of DEGs between H_2O_2 and PBA&NO NP group. (C) Possible mechanism of PBA&NO NP. (D) Cytoplasmic calcium level detected by Fluo-4 AM probe, (E) mitochondrial calcium level detected by Rhod-2 AM probe and Mitotracker co-staining, and (F) mitochondrial membrane potential detected by JC-10 assay. The nuclei were labeled by Hoechst 33258, scale bars, 100 μm. (G) Flow cytometry analysis of HUVECs after different treatments for 24 h using annexin V-FITC and PI assay. The inner image was the percentage of apoptotic cells. (H) WB of ER stress-related protein (XBP-1) and apoptosis-related proteins (BAX, Bcl2 and c-cas3) after different treatments. The concentrations of NO and PBA in the NPs were both 10 μM. Data are presented as mean ± SD (n = 3). $^{**}p < 0.01$, $^{***}p < 0.001$, $^{****}p < 0.0001$.

fluorescence in the NO NP and PBA&NO NP groups proved the successful delivery of NO into cells. However, the red fluorescence from $ONOO^-$ probe significantly intensified in NO NP group, indicating remarkable increase of $ONOO^-$. The results suggested that large portion of NO that were delivered into the cells was turned into RNS under oxidative condition. On the contrary, the bright fluorescence of NO probe with the dimmer fluorescence of $ONOO^-$ probe in the PBA&NO NP treated cells proved that ROS scavenging strategy minimized the generation of harmful RNS.

Over-migration and proliferation of SMCs were regarded as key factors of disruption of vessel homeostasis. Therefore, Transwell assay was performed to assess the selective regulation of different NPs on the migration of HUVECs and HASMCs (Fig. 5D–F). H_2O_2 treatment decreased the migration of HUVECs (an 80% drop), while dramatically promoted the migration of HASMCs (a 300% increase), according to crystal violet staining. Treatment with PBA&NO NP reversed their migration to the similar level of H_2O_2-untreated cells. However, PBA NP or NO NP treatments alone slightly changed the number of migrated cells. These experimental results showed that PBA&NO NP improved NO bioavailability and differentially modulated the behaviors of both HASMCs and HUVECs.

To evaluate the cell growth behaviors, co-culture experiments were conducted to test the competitiveness of HUVECs over HASMCs, which is vital in restoration of vascular homeostasis after injury [44]. Cells pre-stained with different colors were initially seeded at similar density, and continuously co-cultured for 72 h (Fig. 6A). The ratio of HUVECs

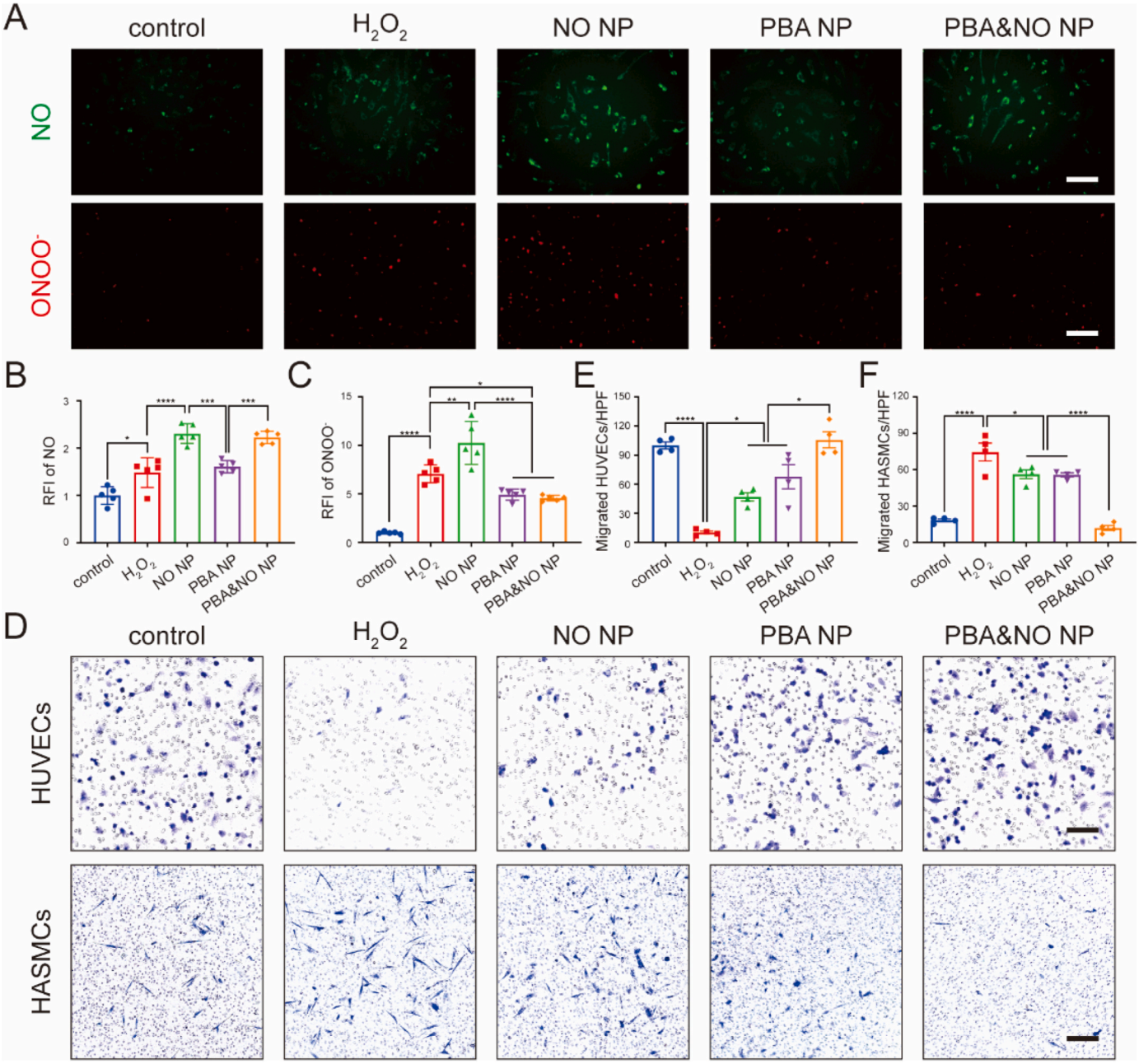

Fig. 5. Regulation of the migration ability in HUVECs and HASMCs by blocking the conversion of NO to $ONOO^-$. (A) Intracellular NO and $ONOO^-$ level detected by DAF-FM DA probe and O58 probe, respectively (scale bars, 100 μm). (B–C) Their relative fluorescence intensity (RFI) was measured. (D) The migration ability was characterized by Transwell assay (scale bars, 100 μm) and (E–F) the number of migrated cells was quantitated in HUVECs and HASMCs. The concentrations of NO and PBA in the NPs were both 10 μM. Data in (B and C) are presented as mean ± SD (n = 5). Data in (E and F) are presented as mean ± SD (n = 4). $^*p < 0.05$, $^{**}p < 0.01$, $^{***}p < 0.001$, $^{****}p < 0.0001$.

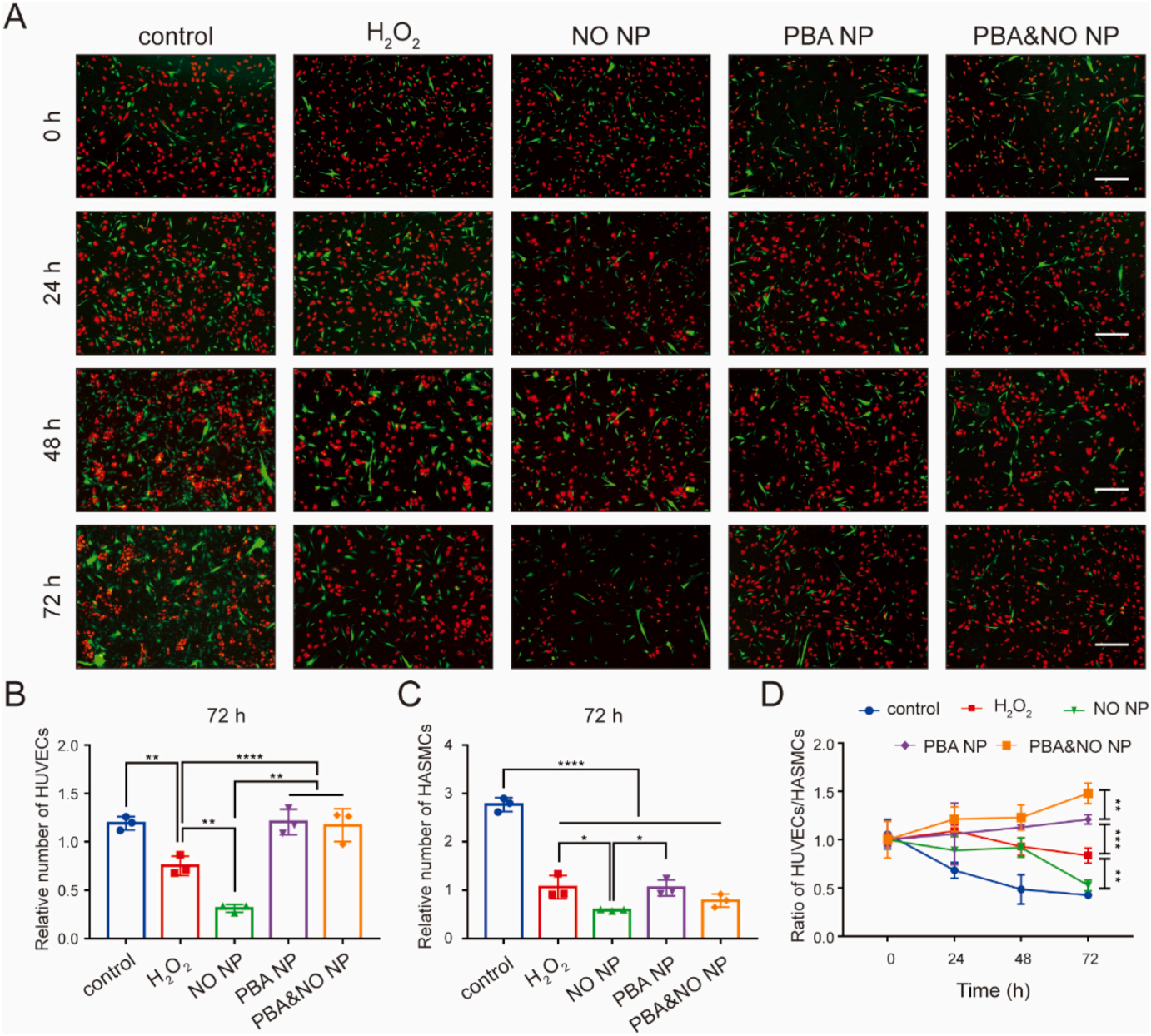

Fig. 6. Improvement of the competitiveness between HUVECs and HAMSCs in the co-culture system. (A) Fluorescence images (scale bars, 100 μm) and (B–D) quantitative results of relative HUVECs number, relative HASMCs number and ratio of HUVECs/HASMCs, respectively. The cells were continuously co-cultured by different treatments for 72 h and images were captured at preset time points. The concentrations of NO and PBA in the NPs were both 10 μM. Data in (B, C and D) are presented as mean ± SD (n = 3). $^{*}p < 0.05$, $^{**}p < 0.01$, $^{***}p < 0.001$, $^{****}p < 0.0001$.

over HASMCs was calculated based on counts of cell number (Fig. 6B–D). Meantime, Relative intracellular NO, ROS and $ONOO^-$ content after different treatments were quantified by flow cytometry at 24, 48 and 72 h (Fig. S7). Interestingly, the number of both kind of cells decreased with treatment of NO NP alone and intracellular NO, ROS and $ONOO^-$ content remained at a high level during 72 h period. This phenomenon indicated that NO supplement alone resulted in the reaction between NO and ROS and the formation of harmful products, $ONOO^-$, under oxidative stress, which lead to more cytotoxicity. On the other hand, the number of HUVECs and the normalized ratio of HUVECs over HASMCs were remarkably increased with treatment of PBA NP and PBA&NO NP, comparing with those of H_2O_2 treated cells. And the intracellular ROS and $ONOO^-$ level were maintained at a lower level in these groups. But, the NO content in PBA&NO NP group was higher than that in PBA NP group. The improvement of competitiveness between HUVECs and HASMCs was also more profound, as demonstrated by higher NO signal during 72 h period and higher ratio of HUVECs over HASMCs on the 3rd day. These results implied that PBA NP had the protective effect on HUVECs but did not have the selective effect like NO. Overall, the ROS-elimination-NO-releasing strategy maximized the bioeffect of NO on selectively promoting HUVECs over HASMCs, leading to higher bioavailability and less toxicity.

2.6. *In vivo inhibitory effect of NPs on restenosis in rats*

Due to the wide applications of percutaneous angioplasty, implants induced damage of endothelium is the main cause of post-treatment events during therapy of CVD [45]. Vascular intima, consisting mostly of endothelial cells, not only evolves as a physical barrier between blood flow and vascular tissue, but also plays an important role in maintaining

vascular homeostasis. The loss of endothelium's intactness and function is the biological basis of many pathological events in CVD. Therefore, fast recovery of functional endothelium was vital in avoiding undesirable side effects, such as restenosis [46].

Herein, a balloon-induced carotid artery injury model was conducted to evaluate the regulatory effects of NPs on endothelium recovery (Fig. 7A). Due to the specific exposure of collagen IV after vascular injury, a collagen IV-targeting peptide was modified onto the NPs to improve site-accumulation of relevant nanomedicines (Fig. S8). The targeting capability in vivo was evaluated with Cy5.5-labeled NPs. 8 h after *i.v.* injection, obvious fluorescence was still observed at sites of vessel injury with t-NPs treatment, much brighter than that of the non-targeted NPs. It demonstrated that peptide decoration could indeed improve accumulation and retention of NPs at injured vascular sites.

Hyperplasia is the key pathological process after endothelium injury, and is the main cause of vascular restenosis and occlusion. Compared with sham group, great thickening of the intimal layer was observed in balloon-injured left carotid arteries 14 days after operation (Fig. 7B). Treatment with t-PBA&NO NP significantly inhibited such abnormal proliferation, with the best reduction in pathological incrassation (Fig. 7C–E). It is of note that NO therapy alone did not achieve remission of intimal thickening. And in some individual cases, the pathological progressions were even worse than operation alone (model group, although without significance after statistical analysis). Our results vividly demonstrated the limitation of NO-based treatments under oxidative stress, in accordance with Zhao and his co-workers' work [26]. It demonstrated the advantages of synergy between anti-ROS and NO therapy in treatment of oxidative stress related diseases.

Consistent with the above results, t-PBA&NO NP showed the best effect on hyperplasia inhibition, as indicated by α-smooth muscle actin (α-SMA) antibody labeling with green fluorescence. Meanwhile, endothelium was labeled by platelet endothelial cell adhesion molecule-1 (CD31) antibody with red fluorescence (Fig. 7F and S9). There were almost no $CD31^+$ signal in the NO therapy alone. But, the synergistic strategy perfectly restored the intactness of endothelium, showing the differential regulation of ECs and SMCs.

To further elucidate such synergic effects, levels of ROS, NO and $ONOO^-$ in tissues were visualized by fluorescent probes and quantified by standard assays, respectively (Fig. 8). It was obvious that NO therapy alone had no effect on reducing intracellular ROS, while significantly increased RNS content. On the contrary, PBA derivates were capable of scavenging abundant ROS after vascular injury, while had little effect on NO concentration. Only the PBA&NO treatment achieved both ROS reduction and NO enhancement, without RNS promotion. These results indicated the present strategy was feasible in improving NO bioavailability and avoiding generation of harmful by-product.

2.7. Biosafety evaluation

To further access the clinical potential, H&E staining and hematological analysis were involved to systemically evaluate the biosafety of different NPs (Figs. S10–11). Negligible pathological changes were observed in H&E slices of major organs. The levels of hematologic parameters, as well as typical biomarkers of hepatic and kidney functions, normal and comparable to those of saline group. Collectively, these NPs treatments showed great biosafety in vivo.

3. Conclusions

In summary, a ROS-responsive & scavenging PBA&NO NP as NO-based therapeutic agents were successfully produced to alleviate endothelial dysfunction. The ROS-triggered ROS elimination effectively alleviated local oxidative stress, ER stress and mitochondrial damage, via antioxidant effect and modulation of Calcium efflux. This strategy minimized conversion of NO into toxic RNS in oxidative microenvironment of vascular injury, thus maximizing NO bioavailability. The NPs greatly increased the competitiveness of HUVECs over HASMCs, improved reendothelialization and achieved excellent anti-restenosis effect in vivo. We believed that this nanomedicine focused on the regulation of endothelial dysfunction provided a promising approach for treatment of vascular injury in several cardiovascular diseases.

4. Experimental methods

4.1. Materials

Isosorbide dinitrate, Ethyl caffeate, 4-hydroxyphenylboronic acid, 2-hydroxypyridine, and 1-(3-Dimethylaminopropyl)-3-ethylcarbodiimide hydrochloride (EDC) were purchased from Energy Chemical Co., Ltd. (Shanghai, China). ,1′-carbonyldiimidazole (CDI) was provided by Macklin Inc. (Shanghai, China). 4-dimethylaminopyridine (DMAP) was purchased from Shanghai Aladdin Biochemical Technology Co., Ltd. (Shanghai, China). Lecithin was purchased from A.V.T Co., Ltd. DSPE-PEG was purchased from Yien Chemical Technology Co., Ltd (Shanghai, China). DSPE-PEG-maleimide was purchased from Xi'an Ruixi Biological Technology Co., Ltd. (Xi'an, China) Coumarin-6 was purchased from Yuanye Biotech (Shanghai, China). Col-IV targeting peptides (CGGGKPLVWL) and scrambled peptides (CGGGLKVPWKL) were purchased from Top-peptide Co., Ltd (Shanghai, China). Antibodies were used in Western blot analysis include: Bax (ab182733, 1:2000, Abcam), Bcl2 (ab182858, 1:2000, Abcam), cleaved caspase3 (c-cas3, 9664, 1:1000, CST), HO-1 (43966, 1:1000, CST), NQO-1, (ab264434, 1:20000, Abcam), XBP1 (MA5-15768, 1:1000, Thermo Fisher), Nrf2 (PA5-88084, 1:500, Thermo Fisher) and β-actin (ab68477, 1:10000, Abcam). The balloons were provided by ZYLOX-TONBRIDGE medical technology Co., LTD. Celltracker dyes (C2927, C7025) were purchased from Thermo Fisher Scientific Inc. (Waltham, MA, USA). DHE, BBoxiProbe® O36, and BBoxiProbe® O58 were purchased from Bestbio biotechnology Co., Ltd (Shanghai, China). Fetal bovine serum was purchased from Zhejiang Baidi Biotechnology Co., Ltd. Fluo-4 AM (40704 ES), Rhod-2 AM (40776 ES), Mitotracker (40742 ES) and Annexin V-FITC/PI apoptosis kit (40302 ES) were purchased from Yeasen Biotechnology Co., Ltd (Shanghai, China). The Griess assay (S0024) and ROS detection kit (S0033S) was purchased from Beyotime Biotechnology Co., Ltd (Shanghai, China). Mitochondrial Membrane Potential Kit (JC-10 Assay) and ABTS Free Radical Scavenging Capacity Assay Kit were purchased from Solarbio Science & Technology Co., Ltd. (Beijing, China).

4.2. Synthesis of β-CD-PBA

According to the previous work, a HP-β-CD-based supramolecular drug (β-CD-PBA) was fabricated [32]. Briefly, ECA and 4-hydroxyphenylboronic acid were added into 10 mL DMF at a molar ratio of 1: 1.15. The suspension was stirred at 100 °C for 8 h and turned into a dark green solution. Excess 4-hydroxyphenylboronic acid was removed by centrifugation and the solvent was removed under rotation evaporation. The product was precipitated from cold ethyl acetate (−20 °C). HP-β-CD and CDI with a molar ratio of 1: 10 were dissolved in anhydrous DCM. After reaction for 1 h, the organic phase was obtained by washing with deionized water three times and drying over Na_2SO_4 and the solvent was removed by rotation evaporation. Then, the obtained CDI-activated HP-β-CD and the phenylborate compound were dissolved in DMF and catalyzed by DMAP for 24 h under room temperature. The product was precipitated from ethyl acetate and dried under vacuum. ^1H NMR, UV–visible and Fourier transform infrared (FT-IR) spectroscopy were conducted to prove the successful synthesis of β-CD-PBA.

4.3. Preparation and characterization of different nanomedicines

The nanoparticles were prepared by a self-assembly/

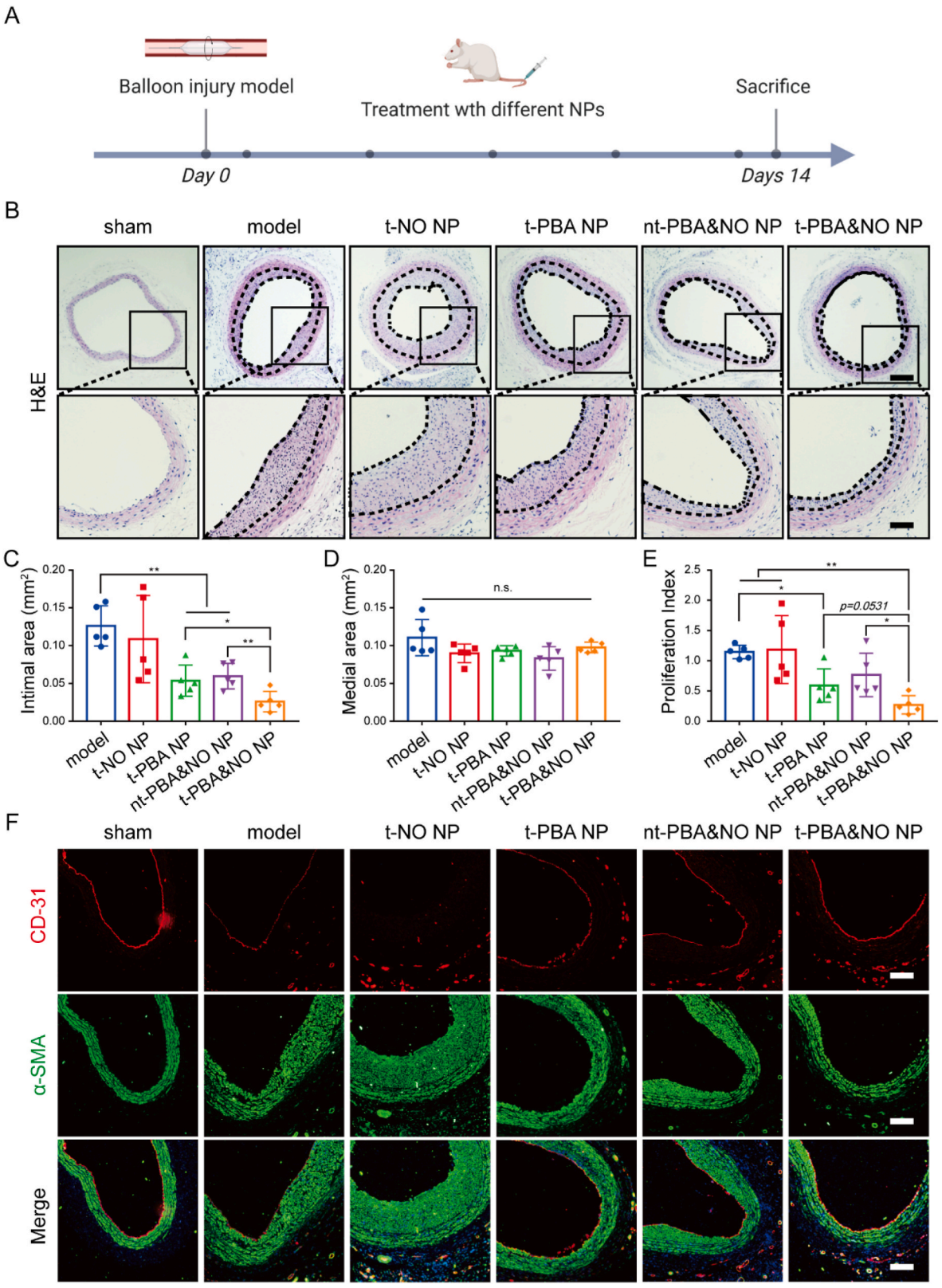

Fig. 7. The anti-restenosis performance of different treatments in vivo. (A) Schematic diagram of the treatments in rats carotid balloon injury model. (B) Representative H&E results after different treatments. Scale bars, (upper panel, 250 μm), (lower panel, 100 μm). (C) Intimal area, (D) medical area and (E) proliferation index after different treatments were quantified according to H&E results. (F) The co-stained results by CD-31 and α-SMA immunofluorescence staining, while nuclei were stained with DAPI (blue), scale bars, 100 μm. Data are presented as mean ± SD (n = 5). *$p < 0.05$, **$p < 0.01$.

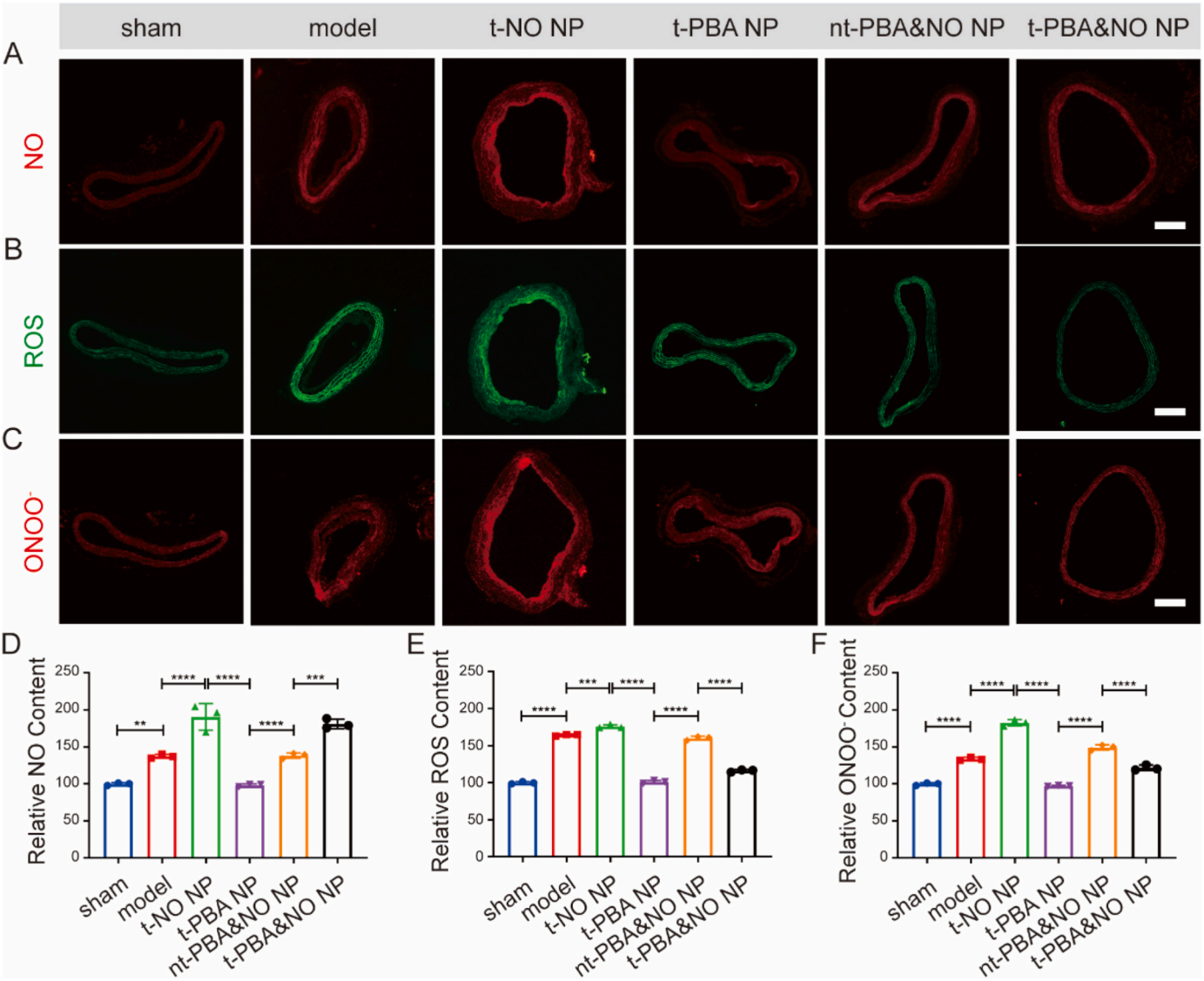

Fig. 8. Immunofluorescence analysis of arterial cross-section after different treatments in carotid balloon injury-induced restenosis model. NO (A), ROS (B) and $ONOO^-$ (C) were stained by corresponding probe, scale bars, 250 μm. Relative NO (D), ROS (E) and $ONOO^-$ (F) content in vascular tissues after different treatments were quantified by fluorescent probe detection kits. Data are presented as mean ± SD (n = 3). $^{**}p < 0.01$, $^{***}p < 0.001$, $^{****}p < 0.0001$.

nanoprecipitation method following previously reported protocol [35]. Briefly, lecithin (3 mg) and DSPE-PEG (4.5 mg) were dissolved in 0.3 mL of ethanol and then dropped into 10 mL of ddH_2O. The mixture was incubated at 65 °C for 2 h, into which 4 mL of cyclodextrin complex solution obtained by mixing β-CD-PBA and ISDN for 30 min under ultrasound was added, and then vigorously stirred at room temperature for 2 h. The remaining organic solvent was removed by vacuum rotary evaporation. Through similar procedures, different formulations of nanoparticles were prepared. Among them, NO NP was nano-encapsulated after ultrasonic mixing of HP-β-CD and ISDN. The unloaded drugs and excess solvent were removed through 30 kDa ultrafiltration membrane and then filtered by 220 μm sterile filter for subsequent biological experiments.

The hydrodynamic diameters, size distribution and zeta potential were measured by Zetasizer Nano-ZS (Malvern instruments). The morphology was characterized by transmission electron microscopy (TEM, HT7700, Hitachi). To test the NO release from ISDN, ISDN (100 μM) was incubated with PBS, cell lysis and cell for 24 h. The NO release at 0 h, 12 h and 24 h were detected by Griess assay, respectively. To test responsive drug release behavior, t-PBA&NO NP was placed into dialysis chamber, which was incubated with 20 mL PBS with or without 1 mM H_2O_2 at 37 °C with shaking at 125 rpm. At preset time point, the release solution was harvested for UV quantitative detection.

4.4. Evaluation of ROS scavenging ability

The ROS scavenging ability was evaluated by 2,2-diphenyl-1- picrylhydrazyl (DPPH) assay and 2,2′-azino-bis (3-ethylbenzothiazoline-6-sulfonic acid) (ABTS) assay. Briefly, 75 μl DPPH (500 μM) was mixed with 25 μl solution with different concentration of PBA (final concentration, 0, 6.25, 12.5, 25, 50, 100, 200 μM). the mixture was incubated in dark for 30 min. Finally, the absorbance at 517 nm was measured and scavenged DPPH was calculated. The ABTS assay was performed under the instruction of its commercially test kit.

4.5. Cell culture

HUVECs and HASMCs were cultured in 25 cm^2 cell culture flasks at 37 °C in a humidified atmosphere with 5% CO_2 and specialized mediums (endothelial cell medium, ECM, smooth muscle cell medium, SMCM)

were purchased from ScienCell Research Laboratories, Inc. (San Diego, CA, USA).

4.6. Evaluation of endocytosis of nanomedicines

HUVECs ($1x10^5$) were cultured in 24-well plates for 24 h. Then, the medium was replaced by flesh ECM with coumarin-6-labeled liposomes. After incubation for preset time period, medium was removed and the cells were washed with PBS. The fluorescence photographs were acquired by fluorescence microscope and the cells were digested by Trypsin for further flow cytometric analysis (BD FACS-CaliburTM).

4.7. Evaluation of cell viability in vitro

HUVECs ($5x10^3$) were cultured in 96-well plates for 24 h. The medium was removed and fresh ECM with different NPs at 10 μM of PBA or/and ISDN. Except the control group, the other groups were treated with 500 μM H_2O_2 to simulate oxidative stress damage. After 24 h, 10% CCK-8 solution was added and incubated for 4 h. The absorbance at 450 nm was measured to determine the cell viability.

Similarly, HUVECs ($1x10^5$) were seeded in 24-well plates. After different treatments for 24 h, the pre-prepared dyeing solution was added and incubated at 37 °C for 30 min without light. Then, the staining effect was observed under fluorescence microscope and images were obtained (live cells, Calcein-AM, green; dead cells, PI, red).

4.8. Evaluation of intracellular ROS, NO and $ONOO^-$ levels in vitro

Intracellular ROS, NO and $ONOO^-$ content were labeled with corresponding specific fluorescent probe, detected by fluorescence microscope, and quantified by flow cytometry. Briefly, HUVECs ($1x10^5$) were cultured in 24-well plates for 24 h. After different treatments for 4 h, the diluted dyeing solution was added. The dyeing solution was prepared by diluting fluorescent probe 1000 times (DHE, a ROS probe, DAF-FM DA probe, a NO probe, BBoxiProbe® O58, a $ONOO^-$ probe), respectively. Then, the cells were incubated at 37 °C for 30 min without light. Subsequently, images were obtained under fluorescence microscopy. For quantitative analysis, the cells were harvested for flow cytometry. Through the similar protocol, Relative intracellular NO, ROS and $ONOO^-$ content after different treatments were quantified by flow cytometry at 24, 48 and 72 h.

4.9. Whole-transcriptome analysis by RNA sequencing (RNA-seq) in HUVECs

Whole-transcriptome analysis by RNA sequencing (RNA-seq) was performed and based on the HUVECs with different treatments. Briefly, HUVECs ($2x10^5$) were cultured in 6-well plates for 24 h. 500 μM H_2O_2 was used for model group and different NPs were added. After incubation for 24 h, the cells were washed with cold PBS for three times and the total RNA was extracted by using TRIzol Plus RNA Purification kit (Invitrogen Thermofisher Scientific, 12183555). According to the protocol, a series of extraction steps were conducted and the RNA was qualified. Then, the total RNA was quantified by Agilent Technologies 2100 bioanalyzer.

4.10. Effects of NPs on ER stress and mitochondria-related cell apoptosis

Cytoplasmic calcium and mitochondrial calcium were detected by calcium-sensitive indicator, Fluo-4 AM and Rhod-2 AM, respectively. Besides, the mitochondria were labeled by Mitotracker. $5x10^4$ cells were seeded in the 24-well plates for 24 h. 500 μM H_2O_2 was used for model group and different NPs were added. After 6 h incubation, medium was removed and the cells were incubated with pre-prepared staining solution (Fluo-4 AM, 1 μM, Rhod-2 AM, 1 μM, and Mitotracker, 100 nM) at 37 °C for another 20 min without light. Subsequently, images were obtained under fluorescence microscope.

The effect of nanomedicines on mitochondrial membrane potential was assessed by JC-10 assay. Briefly, the cells were cultured in the 24-well plates for 24 h and treated with different formulations for another 6 h. According to the protocol, the medium was replaced by the JC-10 staining solution. After 20 min incubation at 37 °C, the cells were washed with blank staining solution 3 times and the mitochondrial membrane potential was visualized by fluorescence microscopy.

For evaluation of nanomedicines' effect on apoptosis, HUVECs ($2x10^5$) were cultured in 6-well plates for 24 h. 500 μM H_2O_2 was used for model group and different NPs were added. After incubation for 24 h, the cells were harvested. According to the Annexin V-FITC/PI apoptosis kit, the percentage of apoptotic cells were quantified by the flow cytometric analysis.

4.11. Evaluation of HUVECs migration ability

To evaluate the migration ability of HUVECs, Transwell assay were performed in the Boyden Chamber and the Costar Transwell apparatus with 8.0-μm pore size (Corning, U.S.A). Briefly, a cell suspension of 200 μl ECM containing 0.5% FBS, and $5x10^4$ cells were added to the upper chamber. Meanwhile, the lower chamber was filled with 500 μl medium containing 10% FBS. 500 μM H_2O_2 was used for model group and different NPs were added. After 8 h incubation, the cells in the upper chamber were removed. The migrated cells were stained with 0.1% crystal violet and photographed by a microscope. Five randomly selected images were used to count the migrated cells by Image J software.

4.12. Western blot analysis in vitro

HUVECs ($2x10^5$) were cultured in 6-well plates for 24 h. 500 μM H_2O_2 was used for model group and different NPs were added. After incubation for 24 h, the cells were harvested for the Western blot analysis. Briefly, the cells were lysed by lysate buffer and the total protein content was quantified by BCA Quantification Kit. Then, the samples were separated by 10% sodium dodecyl sulfate-polyacrylamide gel electrophoresis (SDS-PAGE) followed by being transferred onto the polyvinylidene fluoride (PVDF) membrane. The nonspecific binding was blocked by incubation with 5% non-fat milk for 1 h and the membranes were incubated with primary antibodies at 4 °C overnight. After washing with TBST 3 times, the membranes were hybridized with corresponding secondary antibodies for 1 h. Finally, the results were obtained by chemiluminescence using an enhanced chemiluminescence detection kit and analyzed by Image J software. β-actin was used as internal control protein.

4.13. Co-culture assays of HUVECs and HASMCs in vitro

To further evaluate the regulatory effects of NPs on HUVECs and HASMCs, in vitro co-culture model was established. Firstly, HUVECs and HASMCs were pre-stained with red and green live cell dye for 12 h, respectively. Then, the cells ($4x10^4$ per well, HUVECs: HASMCs, 1:1) were seeded in 24-well plates with ECM, in which 300 μM H_2O_2 and different NPs were added, except for the control group. At the predetermined time points, the cells were photographed by a fluorescence microscope and Image J software was used for subsequent analysis.

4.14. Animals

All in vivo experiments were performed in the guidelines for the care and use of laboratory animals of Animal Care and Use Committee, Zhejiang Academy of Medical Sciences. Healthy male Sprague-Dawley (SD) rats (300–350 g) were purchased from the animal center of Zhejiang Academy of Medical Sciences. Balloon-induced carotid artery injury model in rats was established for in vivo evaluation [47]. Thirty

SD rats were randomly assigned into 6 groups (n = 5, including sham group, model group and groups treated with t-NO NP, t-PBA NP, nt-PBA&NO NP or t-PBA&NO NP, respectively). Different nanomedicines were intravenously administered with 1 mM equivalent drug molecules on days 0, 3, 6, 9, 12. On day 14, rats were euthanized. Blood samples, the left carotid arteries, and major organs were harvested for histological analysis. Balloon injury was not performed in the sham group. Other operations were consistent with those in experimental groups.

4.15. Biodistribution of nanomedicines

To test the targeting capability and biodistribution of NPs, the SD rats were randomly divided into three groups to carry out balloon-induced carotid artery injury surgery. Saline, Cy5.5-nt-NPs, and Cy5.5-t-NPs were intravenously injected, respectively. At 8 h after injection, rats were sacrificed and carotid arteries and major organs (including heart, liver, spleen, lung, and kidney) were harvested for the ex vivo fluorescence photographs under IVIS 50 in vivo imaging system (Perkin Elmer, MA).

4.16. Evaluation of anti-restenosis effect

The left carotid arteries were divided into two segments. One segment was fixed in formalin for paraffin embedding and the cross-sections of arteries were stained with H&E, CD31 (ab222783, Abcam), and α-SMA (ab7817, Abcam). The other segment was harvested for frozen sections. The generation of vascular ROS, NO and $ONOO^-$ was assessed by fluorescent probes labeling. The images were captured by fluorescence microscope and Image J software was used for subsequent analysis. The tissues were homogenized in an ice bath and the supernatant was obtained by centrifugation at 12000 rpm, 4 °C, for 15 min. Then, the ROS, NO and $ONOO^-$ probes were added into the supernatant, respectively (1:1000). The mixtures were incubated at 37 °C for 30 min without light. The fluorescence intensities were measured at Ex510/Em610 for NO, Ex488/Em525 for ROS and Ex516/Em606 for $ONOO^-$, respectively.

4.17. Biosafety evaluation in vivo

To evaluate the biosafety of NPs, blood samples and major organs were collected. The level of hematologic parameters and typical biomarkers of hepatic and kidney functions (ALT, AST, UA, BUN, CR) were tested. The major organs were fixed in formalin and embedded in paraffin for H&E staining.

4.18. Statistical analysis

All experimental data were presented as mean ± standard deviation (SD). GraphPad Prism Software Version 9.0 (San Diego, CA, USA) and Origin (OriginLab Corporation, Northampton, MA, USA) were used for statistical analysis. Comparisons were performed using student's t-test (two groups) or one-way ANOVA analysis with Tukey's post hoc tests (three or more groups). $*p < 0.05$ was considered statistically significant.

Ethics approval and consent to participate

All animal studies were performed in accordance with the relevant regulations, and all protocols are approved by the Institutional Animal Care and Use Committee, Zhejiang Academy of Medical Sciences. Approval No. ZJCLA-IACUC-20030097.

CRediT authorship contribution statement

Jian Li: Writing – review & editing, Writing – original draft, Visualization, Validation, Methodology, Investigation, Formal analysis, Data curation, Conceptualization. **Jvhong Zhang:** Writing – review & editing, Methodology, Investigation. **Pengcheng Yu:** Writing – original draft, Methodology, Investigation, Formal analysis. **Han Xu:** Resources, Investigation. **Meihui Wang:** Project administration, Investigation. **Zhebin Chen:** Methodology, Formal analysis. **Bo Yu:** Methodology, Formal analysis. **Jing Gao:** Methodology, Investigation. **Qiao Jin:** Writing – review & editing, Writing – original draft, Funding acquisition. **Fan Jia:** Writing – review & editing, Writing – original draft, Methodology, Investigation, Funding acquisition, Conceptualization. **Jian Ji:** Supervision, Resources, Funding acquisition. **Guosheng Fu:** Supervision, Resources, Funding acquisition.

Declaration of competing interest

The authors declare that they have no known competing financial interests or personal relationships that could have appeared to influence the work reported in this paper.

Acknowledgments

This work was supported by the National Key Research and Development Program of China (2022YFB3807300), the National Natural Science Foundation of China (51933009, 82370427, 22305219), the Fundamental Research Funds for the Central Universities, China (26-2023-00074), the Natural Science Foundation of Zhejiang Province, China (No.LY20H020005), The Zhejiang Provincial Traditional Chinese Medicine Science and Technology Plan, China (2022ZX012), The Province and Central Administration- Zhejiang Provincial Health Commission, China (WKJ-ZJ-2209).

Appendix A. Supplementary data

Supplementary data to this article can be found online at https://doi.org/10.1016/j.bioactmat.2024.03.010.

References

[1] H. Clark, NCDs: a challenge to sustainable human development, Lancet 381 (9866) (2013) 510–511.
[2] E.J. Benjamin, P. Muntner, A. Alonso, M.S. Bittencourt, C.W. Callaway, A. P. Carson, A.M. Chamberlain, A.R. Chang, S. Cheng, S.R. Das, F.N. Delling, L. Djousse, M.S.V. Elkind, J.F. Ferguson, M. Fornage, L.C. Jordan, S.S. Khan, B. M. Kissela, K.L. Knutson, T.W. Kwan, D.T. Lackland, T.T. Lewis, J.H. Lichtman, C. T. Longenecker, M.S. Loop, P.L. Lutsey, S.S. Martin, K. Matsushita, A.E. Moran, M. E. Mussolino, M. O'Flaherty, A. Pandey, A.M. Perak, W.D. Rosamond, G.A. Roth, U. K.A. Sampson, G.M. Satou, E.B. Schroeder, S.H. Shah, N.L. Spartano, A. Stokes, D. L. Tirschwell, C.W. Tsao, M.P. Turakhia, L.B. VanWagner, J.T. Wilkins, S.S. Wong, S.S. Virani, Heart disease and stroke statistics-2019 update: a report from the American heart association, Circulation 139 (10) (2019) e56–e528.
[3] Y. Han, K. Huang, Q.-P. Yao, Z.-L. Jiang, Mechanobiology in vascular remodeling, Natl. Sci. Rev. 5 (6) (2018) 933–946.
[4] J.K. Freed, D.D. Gutterman, Mitochondrial reactive oxygen species and vascular function less is more, Arterioscler. Thromb. Vasc. Biol. 33 (4) (2013) 673–675.
[5] M. Hulsmans, P. Holvoet, The vicious circle between oxidative stress and inflammation in atherosclerosis, J. Cell Mol. Med. 14 (1–2) (2010) 70–78.
[6] R. Rubinshtein, J.T. Kuvin, M. Soffler, R.J. Lennon, S. Lavi, R.E. Nelson, G. M. Pumper, L.O. Lerman, A. Lerman, Assessment of endothelial function by non-invasive peripheral arterial tonometry predicts late cardiovascular adverse events, Eur. Heart J. 31 (9) (2010) 1142–1148.
[7] H.L. Qian, S.Y. Chen, F. Jia, W.P. Huang, J. Wang, K.F. Ren, G.S. Fu, J. Ji, "Spongy skin" as a robust strategy to deliver 4-octyl itaconate for conducting dual-regulation against in-stent restenosis, Biomaterials (2023) 296.
[8] B.F. Zhao, Y.P. Zhuang, Z.M. Liu, J.Y. Mao, S.T. Qian, Q.Y. Zhao, B.L. Lu, X.Y. Mao, L.C. Zhang, Y.G. Zhang, W.G. Cui, X.M. Sun, Regulated extravascular microenvironment via reversible thermosensitive hydrogel for inhibiting calcium influx and vasospasm, Bioact. Mater. 21 (2023) 422–435.
[9] B.Y. Lu, X. Han, A.S. Zhao, D. Luo, M.F. Maitz, H.H. Wang, P. Yang, N. Huang, Intelligent H2S release coating for regulating vascular remodeling, Bioact. Mater. 6 (4) (2021) 1040–1050.
[10] X.C. Pi, L. Xie, C. Patterson, Emerging roles of vascular endothelium in metabolic homeostasis, Circ. Res. 123 (4) (2018) 477–494.
[11] S. Godo, H. Shimokawa, Endothelial functions, Arterioscler. Thromb. Vasc. Biol. 37 (9) (2017) e108–e114.

[12] X.F. Zhou, Y.Q. Jiang, Y.W. Wang, L.E. Fan, Y.H. Zhu, Y.F. Chen, Y.R. Wang, Y. Y. Zhu, H.K. Wang, Z.H. Pan, Z.B. Li, X.L. Zhu, R.Z. Ren, Z. Ge, D.W. Lai, E.Y. Lai, T. Chen, K. Wang, P. Liang, L.F. Qin, C.Q. Liu, C. Qiu, M. Simons, L.Y. Yu, Endothelial FIS1 DeSUMOylation protects against hypoxic pulmonary hypertension, Circ. Res. 133 (6) (2023) 508–531.
[13] C. Farah, L.Y.M. Michel, J.L. Balligand, Nitric oxide signalling in cardiovascular health and disease, Nat. Rev. Cardiol. 15 (5) (2018) 292–316.
[14] D. Tousoulis, A.M. Kampoli, C. Tentolouris, N. Papageorgiou, C. Stefanadis, The role of nitric oxide on endothelial function, Curr. Vasc. Pharmacol. 10 (1) (2012) 4–18.
[15] U. Förstermann, T. Münzel, Endothelial nitric oxide synthase in vascular disease -: from marvel to menace, Circulation 113 (13) (2006) 1708–1714.
[16] P.M. Vanhoutte, Y. Zhao, A. Xu, S.W. Leung, Thirty years of saying NO: sources, fate, actions, and misfortunes of the endothelium-derived vasodilator mediator, Circ. Res. 119 (2) (2016) 375–396.
[17] S.Y. Chen, F. Jia, L.Y. Zhao, F.Y. Qiu, S.H. Jiang, J. Ji, G.S. Fu, Electrospun fiber membrane with asymmetric NO release for the differential regulation of cell growth, Bio-Des. Manuf. 4 (3) (2021) 469–478.
[18] Q. Qin, M. Chen, N. Yu, K. Yao, X. Liu, Q. Zhang, Y. Wang, J. Ji, K. Wang, F. Jia, Macromolecular carrier with long retention and body-temperature triggered nitric oxide release for corneal alkali burn therapy via leptin-related signaling, Nano Today 54 (2024).
[19] M.N. Sack, F.Y. Fyhrquist, O.J. Saijonmaa, V. Fuster, J.C. Kovacic, Basic biology of oxidative stress and the cardiovascular system Part 1 of a 3-Part Series, J. Am. Coll. Cardiol. 70 (2) (2017) 196–211.
[20] J.S. Beckman, Oxidative damage and tyrosine nitration from peroxynitrite, Chem. Res. Toxicol. 9 (5) (1996) 836–844.
[21] R.J. Gryglewski, R.M.J. Palmer, S. Moncada, Superoxide anion is involved in the breakdown of endothelium-derived vascular relaxing factor, Nature 320 (6061) (1986) 454–456.
[22] D.F. Hu, Y.Y. Deng, F. Jia, Q. Jin, J. Ji, Surface charge switchable supramolecular nanocarriers for nitric oxide synergistic photodynamic eradication of biofilms, ACS Nano 14 (1) (2020) 347–359.
[23] C. Hetz, The unfolded protein response: controlling cell fate decisions under ER stress and beyond, Nat. Rev. Mol. Cell Biol. 13 (2) (2012) 89–102.
[24] T. Minamino, M. Kitakaze, ER stress in cardiovascular disease, J. Mol. Cell. Cardiol. 48 (6) (2010) 1105–1110.
[25] T. Minamino, I. Komuro, M. Kitakaze, Endoplasmic reticulum stress as a therapeutic target in cardiovascular disease, Circ. Res. 107 (9) (2010) 1071–1082.
[26] T. Hao, M. Qian, Y.T. Zhang, Q. Liu, A.C. Midgley, Y.P. Liu, Y.Z. Che, J.L. Hou, Q. Zhao, An injectable dual-function hydrogel protects against myocardial ischemia/reperfusion injury by modulating ROS/NO disequilibrium, Adv. Sci. 9 (15) (2022).
[27] Z. Wang, N. Yang, Y. Hou, Y. Li, C. Yin, E. Yang, H. Cao, G. Hu, J. Xue, J. Yang, Z. Liao, W. Wang, D. Sun, C. Fan, L. Zheng, L-Arginine-Loaded gold nanocages ameliorate myocardial ischemia/reperfusion injury by promoting nitric oxide production and maintaining mitochondrial function, Adv. Sci. 10 (26) (2023).
[28] J. Mu, C. Li, Y. Shi, G. Liu, J. Zou, D.-Y. Zhang, C. Jiang, X. Wang, L. He, P. Huang, Y. Yin, X. Chen, Protective effect of platinum nano-antioxidant and nitric oxide against hepatic ischemia-reperfusion injury, Nat. Commun. 13 (1) (2022).
[29] T. Zhao, W. Wu, L. Sui, Q. Huang, Y. Nan, J. Liu, K. Ai, Reactive oxygen species-based nanomaterials for the treatment of myocardial ischemia reperfusion injuries, Bioact. Mater. 7 (2022) 47–72.
[30] Z. Zhang, R. Dalan, Z. Hu, J.W. Wang, N.W.S. Chew, K.K. Poh, R.S. Tan, T. W. Soong, Y. Dai, L. Ye, X. Chen, Reactive oxygen species scavenging nanomedicine for the treatment of ischemic heart disease, Adv. Mater. 34 (35) (2022).
[31] T. Wu, X. Chen, Y. Wang, H. Xiao, Y. Peng, L. Lin, W. Xia, M. Long, J. Tao, X. Shuai, Aortic plaque-targeted andrographolide delivery with oxidation-sensitive micelle effectively treats atherosclerosis via simultaneous ROS capture and anti-inflammation, Nanomedicine 14 (7) (2018) 2215–2226.
[32] F. Jia, B. Yu, J. Li, F. Cai, G. Fu, Q. Jin, J. Ji, Supramolecular nano-assembly of caffeate-strengthened phenylboronic ester with multistep ROS scavenging ability for targeted therapy of acute kidney injury, Adv. Healthcare Mater. 12 (30) (2023) 2301615.
[33] Y.-T. Li, S.-T. Sheng, B. Yu, F. Jia, K. Wang, H.-J. Han, Q. Jin, Y.-X. Wang, J. Ji, An ROS-responsive antioxidative macromolecular prodrug of caffeate for uveitis treatment, Chinese J. Polym. Sci. 40 (9) (2022) 1101–1109.
[34] J. Zhao, J.Y. Fu, F. Jia, J. Li, B. Yu, Y. Huang, K.F. Ren, J. Ji, G.S. Fu, Precise regulation of inflammation and oxidative stress by ROS-responsive prodrug coated balloon for preventing vascular restenosis, Adv. Funct. Mater. 33 (30) (2023).
[35] Y. Dou, Y. Chen, X.J. Zhang, X.Q. Xu, Y.D. Chen, J.W. Guo, D.L. Zhang, R.B. Wang, X.H. Li, J.X. Zhang, Non-proinflammatory and responsive nanoplatforms for targeted treatment of atherosclerosis, Biomaterials 143 (2017) 93–108.
[36] A.-L. Levonen, M. Inkala, T. Heikura, S. Jauhiainen, H.-K. Jyrkkänen, E. Kansanen, K. Määttä, E. Romppanen, P.i. Turunen, J. Rutanen, S. Ylä-Herttuala, Nrf2 gene transfer induces antioxidant enzymes and suppresses smooth muscle cell growth in vitro and reduces oxidative stress in rabbit aorta in vivo, Arterioscler. Thromb. Vasc. Biol. 27 (4) (2007) 741–747.
[37] A. Cuadrado, G. Manda, A. Hassan, M.J. Alcaraz, C. Barbas, A. Daiber, P. Ghezzi, R. León, M.G. López, B. Oliva, M. Pajares, A.I. Rojo, N. Robledinos-Antón, A. M. Valverde, E. Guney, H.H.H.W. Schmidt, M.C. Michel, Transcription factor NRF2 as a therapeutic target for chronic diseases: a systems medicine approach, Pharmacol. Rev. 70 (2) (2018) 348–383.
[38] J.R. Friedman, G.K. Voeltz, The ER in 3D: a multifunctional dynamic membrane network, Trends Cell Biol. 21 (12) (2011) 709–717.
[39] D. Ron, P. Walter, Signal integration in the endoplasmic reticulum unfolded protein response, Nat. Rev. Mol. Cell Biol. 8 (7) (2007) 519–529.
[40] E. Bertero, C. Maack, Calcium signaling and reactive oxygen species in mitochondria, Circ. Res. 122 (10) (2018) 1460–1478.
[41] A.A. Rowland, G.K. Voeltz, Endoplasmic reticulum–mitochondria contacts: function of the junction, Nat. Rev. Mol. Cell Biol. 13 (10) (2012) 607–615.
[42] J.R. Friedman, L.L. Lackner, M. West, J.R. DiBenedetto, J. Nunnari, G.K. Voeltz, Demonstrates that mitochondrial division occurs at positions where ER tubules contact mitochondria, and that contact and constriction occurs prior to recruitment of the division machinery, Science 334 (6054) (2011) 358–362.
[43] Z. Yang, Y. Yang, L. Zhang, K. Xiong, X. Li, F. Zhang, J. Wang, X. Zhao, N. Huang, Mussel-inspired catalytic selenocystamine-dopamine coatings for long-term generation of therapeutic gas on cardiovascular stents, Biomaterials 178 (2018) 1–10.
[44] H. Hao, Y. Xue, Y. Wu, C. Wang, Y. Chen, X. Wang, P. Zhang, J. Ji, A paradigm for high-throughput screening of cell-selective surfaces coupling orthogonal gradients and machine learning-based cell recognition, Bioact. Mater. 28 (2023) 1–11.
[45] J.W. Jukema, T.A. Ahmed, J.J. Verschuren, P.H. Quax, Restenosis after PCI. Part 2: prevention and therapy, Nat. Rev. Cardiol. 9 (2) (2011) 79–90.
[46] R. Wang, J. Lu, J.S. Yin, H. Chen, H.M. Liu, F. Xu, T.T. Zang, R.D. Xu, C.G. Li, Y. Z. Wu, Q.L. Wu, X. Fei, M.F. Zhu, L. Shen, J.B. Ge, A TEMPOL and rapamycin loaded nanofiber-covered stent favors endothelialization and mitigates neointimal hyperplasia and local inflammation, Bioact. Mater. 19 (2023) 666–677.
[47] J. Li, F. Jia, Z.B. Chen, J. Lin, Q.B. Lv, Y. Huang, Q. Jin, Y.X. Wang, G.S. Fu, J. Ji, Targeted delivery of liver X receptor agonist to inhibit neointimal hyperplasia by differentially regulating cell behaviors, Biomater. Sci. 10 (22) (2022) 6354–6364.